Invariant chain regulates endosomal fusion and maturation through the SNARE Vti1b

Dominik Frei*[1], Azzurra Margiotta*[1], Marita Borg Distefano[1],
Mohamed Moulefera[2], Lennert Janssen[3], Jacques Thibodeau[2], Jacques
Neefjes[3] and Oddmund Bakke[1#]

*Equal contribution.

[1] Department of molecular Biosciences, University of Oslo, Oslo, Norway.

[2] Université de Montréal, Laboratoire d'immunologie moléculaire, Département de microbiologie, Infectiologie et Immunologie, Montreal, Canada

[3] Department of Cell and Chemical Biology, Oncode Institute, Leiden University Medical Center LUMC, Leiden, The Netherlands

[#] Corresponding author email:oddmund.bakke@ibv.uio.no

Running title: Invariant chain interacts with Vti1b

Abstract

Invariant chain (Ii) is an important multifunctional player in the regulation of adaptive immune responses and is responsible for several cellular functions related to MHCI and MHCII antigen loading and antigen presentation. While regulating endosomal trafficking of MHCII and other proteins that bind to Ii, this molecule is able to influence the endosomal pathway delaying the maturation of endosomes to the late endosomal loading compartments. When expressed in cells Ii is found to increase endosomal size, but the mechanisms for this is not known. We used RNAi silencing to identify SNARE proteins controlling Ii induced increase of endosomal size and delay of the endosomal pathway. Ii was found to interact with the SNARE protein Vti1b. Vti1b localized at the contact sites of fusing Ii positive endosomes and a tailless Ii was able to relocate Vti1b to the plasma membrane. Furthermore, silencing Vti1b, abrogated the delay in endosomal maturation induced by Ii expression. In conclusion, Ii interacts with Vti1b and this interaction is fundamental for Ii-mediated alteration of the endosomal pathway. We propose that Ii, by interacting with SNAREs, in particular Vti1B in the biosynthetic pathway of antigen presenting cells, is able to assemble SNARE directed fusion partners in the early part of the endosomal pathway that lead to a slower endosomal maturation for efficient antigen processing and antigen loading.

Keywords: endosomal fusion/Ii/Vti1b/SNAREs/MHCII

61

62

63

Introduction

64

65   Professional antigen presenting cells like dendritic cells and B cells express major

66 histocompatibility complex class II (MHCII) and associated molecules in the MHC region and

67 invariant chain (Ii, or CD74) located on a different chromosome (Genuardi and Saunders 1988).

68 While MHCII is a polymorphic protein, Ii is a non-polymorphic type II transmembrane protein

69 that forms complexes by self-trimerization and binding to MHC class II (reviewed in

70 (Landsverk, Bakke, and Gregers 2009). Ii is mainly expressed in antigen presenting cells

71 (APCs) and has a prominent role sorting associated molecules to the endosomal pathway

72 (reviewed in (Schroder 2016)). Importantly, Ii, which contains two efficient leucine based

73 endosomal sorting signals, facilitates the exit of MHC class II from the endoplasmic reticulum

74 (ER) in antigen-presenting cells and mediates rapid transport of the MHCII/Ii complex to the

75 endosomal pathway where the antigen is efficiently loaded (Bremnes et al. 1994; Bakke and

76 Dobberstein 1990; Elliott et al. 1994; Bikoff et al. 1993; Neefjes and Ploegh 1992). In addition,

77 Ii delayed transport from Rab5 positive early endosomes (EE) to late Rab7a positive

78 endosomes (LE) (Gorvel et al. 1995). Ii also induced fusion of early endosomes creating

79 enlarged endosomes (Pieters, Bakke, and Dobberstein 1993; Romagnoli et al. 1993). These

80 enlarged endosomes were able to mature normally, however, with a prolonged residence time

81 in EE (presence of EEA1 and Rab5) before the endosomes switched to late, acidic Rab7a and

82 Lamp1 positive multivesicular endosomes and lysosomes (Stang and Bakke 1997; Landsverk

83 et al. 2011).

84   Most membrane fusion events in the cell require SNARE (soluble N-ethylmaleimide-

85 sensitive-factor (NSF) attachment protein (SNAP) receptor) proteins (reviewed in (Jahn and

86 Scheller 2006)). All SNAREs share the conserved SNARE motif of 60-70 amino acids

87 (Weimbs et al. 1997) and generally contain a transmembrane domains; however, some are

88 anchored to membranes by lipid modifications. There are several types of SNARE domains:

89 R-SNAREs contribute an arginine residue to the binding layer of the assembled complex, while

90 Q-SNAREs have conserved glutamine residues (Fasshauer et al. 1998). Q-SNAREs are further

91 subdivided into Qa-, Qb- and Qc-SNAREs depending on their position in the complex. One

92 SNARE domain of each class is required to form the complex. The formation of this complex

93 provides the driving power necessary for membrane fusion.

94   Interestingly, although PI3K inhibitors block homotypic fusion of early endosomes (Jones and
95   Clague 1995; Powis et al. 1994), this is not the case for Ii-positive endosomes (Nordeng et al.
96   2002). This indicates that the Ii mediated fusion mechanism differ from the standard early
97   endosomal fusion machinery. The Ii induced fusion of endosomes was, however, inhibited by
98   NEM suggesting that SNARE molecules were involved in this process. After failed rounds of
99   searching for Ii associated proteins explaining the trafficking effects by two-hybrid screens and
100 coimmunoprecipitations experiments, we set out to test the involvement of every individual
101 SNARE protein in the Ii specific endosomal fusion events.

102   Our siRNA screen and subsequent verification identified the Q-SNARE Vti1b as a
103 plausible candidate. Vti1b depletion reduced Ii-induced endosomal size, indicating a functional
104 role in this process. This was further substantiated by a co-isolation of Vti1b with Ii. Vti1b was
105 found enriched at contact sites between Ii-positive endosomes and present at the fusion pore.
106 As a further proof, depletion of Vti1b abrogated the effect of Ii-induced delay in endosomal
107 maturation. These data suggest that Vti1b is an essential element in the regulation of the
108 endosomal pathway by Ii.

109

Results

Ii regulates endosomal maturation in antigen presenting cells.

112   In our earlier studies the Ii induced endosomal maturation delay was measured as a
113 delayed entry from Rab5 positive to Rab7 positive endosomes (Gorvel et al. 1995) or a
114 prolonged EE phase (Landsverk et al. 2011) in non-antigen presenting cells without the MHC
115 domain molecules. If Ii has a similar regulatory role on endosomal maturation in cells
116 containing the full MHC II antigen presenting machinery removal of Ii should speed up
117 endosomal maturation. To test for this, we generated, using CRISPR-Cas9, human antigen-
118 presenting cell lines lacking Ii (Ii KO) (see M&M). We first followed progression of the
119 fluorescent fluid phase marker 8-hydroxypyrene-1,3,6-trisulphonate (HPTS) in human
120 lymphoblast Raji cells either expressing the Cas9 enzyme (control) or Ii KO by measuring the
121 time for a HPTS to colocalize with acidic lysotracker red (LTR) late endosomes. In Ii KO cells,
122 fluid phase marker HPTS reached lysotracker red (LTR) late endosomes faster than in the
123 control cells (Figure 1A). 1 hour after addition of HPTS the colocalization with LTR was 45%
124 in the Ii KO cells while in the corresponding control cells, this was 30% indicating that the KO
125 of Ii in the Raji cells causes a significant faster endosomal maturation. Meljuso cells naturally
126 express Ii and MHCII and are a popular model system for studying antigen presentation. HPTS

4

127 colonization with LTR was followed over time in control and Ii KO MelJuSo cells for up to

128 200 min (Fig 1B). At this time point, in the Ii KO cells about 50% of LTR colocalized with

129 HPTS, compared to only 30% in control cells. The entry of HPTS into late endosomal

130 compartments was again significantly faster in Ii KO cells. This suggests that Ii regulates

131 endosomal maturation not only in model fibroblast-like cell lines transfected with Ii, but also

132 in antigen presenting cells that contain the full MHCII-related antigen processing and

133 presentation machinery.

134

135 **Vti1b is involved in Ii-mediated endosome enlargement.**

136   When Ii was expressed in non-antigen presenting cells, the size of the endosomal

137 compartments strongly increased (Pieters, Bakke, and Dobberstein 1993; Romagnoli et al.

138 1993). In fact, there was a direct correlation between the size increase and Ii-expression levels

139 (Nordeng et al. 2002). Both the delayed maturation and the endosomal expansion was

140 dependent on Ii trimerization and suggested that these effects were caused by the same

141 mechanism (Nordeng et al. 2002; Gregers et al. 2003). NEM is a chemical compound that

142 block amongst others SNARE proteins. Since NEM inhibited Ii driven effects on the

143 endosomal pathway, we proposed a contribution of SNAREs (Nordeng et al. 2002).

144   To test for SNAREs involved in Ii-mediated endosome enlargement, we silenced all

145 individual SNAREs in the M1 fibroblast cell line, stably transfected with Ii under the control

146 of a heavy-metal inducible promoter (M1 pMep4-Ii, (Nordeng et al. 2002)). The M1 wild type

147 cell line is negative for Ii and the MHCII proteins but the cell line has been employed

148 extensively to study endosomal dynamics and antigen presentation by transfecting in immune

149 genes (Roche et al. 1993; Stang and Bakke 1997; Skjeldal et al. 2012; Sand et al. 2014; Haugen

150 et al. 2017). Ii transport to Ii positive endosomes was visualized by adding fluorescently tagged

151 antibody recognizing the extracellular/luminal domain of Ii, and the size of Ii-positive

152 endosomes was analysed by confocal microscopy (Figure 2A).

153   As a test for our screening system we employed some of the known inhibitors of early

154 endosome fusion. The MAP kinase inhibitor SB203580 (Cuenda et al. 1995) was used to block

155 Rab5 activation and Wortmannin to inhibit PI3K activity (Wymann et al. 1996). As shown

156 earlier (Nordeng et al. 2002), wortmannin did not inhibit formation of enlarged endosomes (Fig

157 2B). MAP kinase activity was also not essential since SB203580 could not stop the formation

158 of the enlarged endosomes (Fig 2B). However, N-ethylmaleimide (NEM), a general inhibitor

159 of SNARE function, significantly reduced Ii-mediated endosome enlargement by about 50%

160 (Fig 2B), in line with earlier results from cell free studies (Nordeng et al. 2002).

161   To screen for specific SNARE proteins involved in Ii-mediated endosome enlargement,

162 inducible M1 pMep4-Ii cells were transfected with pools of siRNAs (four oligos per target

163 gene) targeting 40 individual human SNAREs. Three days post-transfection, cells were

164 analysed by 3D confocal microscopy to determine the degree of endosome enlargement upon

165 Ii expression. This screen showed that silencing Vti1b counteracted the Ii induced endosome

166 enlargement by 50%. Validation with individual siRNAs for Vti1b showed an even stronger

167 inhibitory effect for two out of the four siRNAs (Fig 2C). Western blot analyses of cells

168 transfected with these siRNAs confirmed a significantly reduced level of the Vti1b target

169 protein (Fig 2D-E).

170 These experiments suggest that depletion of Vti1b inhibits the Ii induced formation of enlarged

171 endosomes.

172

173 Silencing of Vti1b specifically reduces Ii-mediated endosome enlargement

174   Given the effect of Vti1b in the regulation of the size of Ii-positive endosomes, we

175 evaluated whether the depletion of this SNARE also interfered with endosomes enlarged by

176 other means than expression of Ii. A well-known method for expanded early endosomes is to

177 express the active mutant of Rab5 (Rab5Q79L) (Stenmark et al. 1994; Wegner et al. 2010). M1

178 pMep4-Ii cells were transfected with control siRNA or siRNA targeting Vti1b and

179 subsequently either treated with $CdCl_2$ to induce Ii expression, (inducible metallothionine

180 promotor) (Fig 3A, top row) or transfected with EGFP-Rab5Q79L (Fig 3A, bottom row).

181 Images were acquired and the size of Ii- or Rab5Q79L-positive endosomes was determined

182 (Fig 3B). Silencing of Vti1b with either of the two siRNAs reduced Ii-mediated endosome

183 expansion by approximately 70% (Fig 3B). On the other hand, Vti1b depletion did not affect

184 the size of Rab5Q79L-positive endosomes, showing that Vti1b is not essential for endosome

185 enlargement of early endosomes induced by active Rab5. To study this process further we

186 quantified the number of endosomes per cell in the above experiment and observed that the

187 silencing of Vti1b significantly increased the number of endosomes after Ii expression (Fig

188 3C). On the other hand, silencing of Vti1b had no effect on the number of endosomes after

189 overexpression of Rab5Q79L (Fig 3C) The above measurements suggest that Vti1b effect is

190 not a general requirement for enlarging early endosomes, but more specific for the Ii induced

191 endosomal expansion.

6

192

Vti1b localized to contact sites between Ii-positive endosomes during their fusion

194   Given the well documented role of SNARE proteins in membrane fusion, we decided

195 to evaluate the localization of Vti1b in M1 pMep4-Ii cells transfected with Ii and Vti1b-

196 mCitrine. Interestingly, cells expressing Vti1b-mCitrine showed that this SNARE protein is

197 localized at the contact sites between Ii-positive endosomes (Fig 4A, Movie EV1, see also 4B

198 top row for fixed cells). In particular, Vti1b-mCitrine was detected directly at the opening

199 fusion pore between two Ii-positive endosomes (Fig 4A, Movie EV1). Moreover, Vti1b-

200 mCitrine was localized in intense microdomains on endosomes with these domains often found

201 at the contact sites between two Ii-positive endosomes. As a control we used again mCherry-

202 Rab5Q79L induced enlarged endosomes (Fig 4B bottom row). Quantification of the frequency

203 with which Vti1b localized at the contact sites showed that Vti1b accumulated at about 80% of

204 the contact sites between Ii-positive endosomes whereas Vti1b localized to this contact zone in

205 40% of the recorded interaction sites between Rab5Q79L-positive endosomes (Fig 4C). This

206 shows that Vti1b is recruited more often to the contact site of fusing Ii-positive endosomes as

207 compared to Rab5Q79L-positive endosomes (Fig 4C). Furthermore, we also evaluated the

208 localization of endogenous Vti1b in M1 pMep4-Ii cells where Ii has been induced and

209 endosomes were enlarged (Fig 4D). Similarly, to the transfected Vti1b-mCitrine fusion protein,

210 immunofluorescence of endogenous Vti1b showed its localization at the contact sites of Ii-

211 positive endosomes (Fig 4D). This was also studied in the Meljuso cells, and again Vti1b

212 localized to contact sites between Ii-positive endosomes (Fig 4E), indicating that Vti1b

213 associated with invariant chain at endosomal contact sites also in professional antigen

214 presenting cells. In Meljuso cells the endosomes were not enlarged showing that Vti1b

215 localization was not restricted to Ii induced enlarged endosomes.

216

Vti1b interacts with Ii

218   As Vti1b has a role in the regulation of the Ii-mediated endosomal enlargement and

219 colocalize with Ii, we tested, whether this SNARE could interact with Ii. Firstly, we transfected

220 either EGFP (as a negative control) or Vti1b-mCitrine into M1 pMep4-Ii cells. The expression

221 of Ii was induced by $CdCl_2$ treatment overnight and then we performed a co-IP experiment

222 using anti-GFP nanobodies. We evaluated the presence of Ii in the eluates by Western blot (Fig

223 5A). We observed a band for Ii after immunoprecipitation of Vti1b-mCitrine with anti-GFP

224 antibodies but not for the control EGFP (Fig 5A) showing that Vti1b interacts with Ii. In order

225 to further elucidate the interaction between Vti1b and Ii, we transfected Vti1b-mCitrine and

226   His-tagged Ii wt or Ii lacking the cytosolic tail (IiΔ27) in HeLa cells. As a negative control we

227   used cells co-transfected with EGFP and Ii wt. Then we performed a co-immunoprecipitation

228   assay with anti-GFP nanobodies (Fig 5B). Interestingly, Vti1b-mCitrine interacted with full-

229   length Ii but also with IiΔ27 (Fig 5B), showing that the cytoplasmic tail of Ii is dispensable for

230   binding to Vti1b.

231

Tailless Invariant chain relocates Vti1b to the plasma membrane

233   Vti1b contains a very short luminal domain (3 amino acids) and a long cytoplasmic tail

234   (Brunger 2005) whereas Ii has a short (30 amino acids) cytoplasmic domain and a long luminal

235   domain (Schroder 2016). Ii without a cytoplasmic tail is known to target invariant chain to the

236   plasma membrane (PM) (Bakke and Dobberstein 1990).

237   To characterize the localization of these two associated proteins, we expressed the

238   tailless Ii with a hexahistidine tag, (His-Ii Δ27) and Vti1b-mCitrine in HeLa cells and as control

239   the same set up with full length Ii. As shown in Figure 6, Vti1b with full-length Ii was located

240   in intracellular vesicles including endosomes positive for Ii. However, when Vti1b was

241   expressed with Ii Δ27, a large fraction of Vti1b colocalized with Ii Δ27 at the PM. Since Vti1b

242   was found to bind both Ii wild type and Ii Δ27, this suggest that these two molecules are

243   associated in the biosynthetic pathway and that Vti1b is actively sorted by Ii to the endosomal

244   pathway.

245

The influence of Ii KO on Vti1b distribution in antigen presenting cells.

247   In the intracellular trafficking experiments above we transfected Ii and mutants into

248   cells lacking MHCII and associated genes (M1 and Hela cells). Meljuso cells, however, express

249   endogenously the proteins involved in MHCII loading including MHCII, Ii and HLA-DM

250   (Elliott and Neefjes 2006). MHCII may change the activities of Ii on endosomal maturation

251   and expansion. To test this, we transfected Vti1b-mCitrine into Meljuso Ii KO and Meljuso wt

252   cells followed by fixation and labelling with anti-CI-M6PR antibody that labels trans-Golgi

253   network (TGN) and endosomes (Fig 7). Interestingly, Vti1b-mCitrine colocalized more with

254   CI-M6PR in the Ii KO cells as compared with the wild type (Fig 7A, for quantitation, Figure

255   7B). We also evaluated the number of vesicles positive for Vti1b-mCitrine which was

256   drastically reduced with about 40 vesicles/cell in the Ii KO cells as compared an average of

257   240 vesicles/cell for the wild type (Fig 7C). The volume of the CI-M6PR positive structures,

258   in the Ii KO and wild type Meljuso cells were not significantly different (Fig 7D). As shown

259   in Figure 7 we were able to rescue the phenotype by transfecting cDNA for Ii into the KO cells

8

260   indicating that the altered intracellular distribution of Vti1b is indeed caused by the Ii KO and

261   not by an off target effect.

262   The CI-M6PR localizes in the trans-Golgi, plasma membrane and the late endosomal

263   pathway (Hille-Rehfeld 1995). To firmly establish the localization of Vti1b in the Meljuso Ii

264   KO, we also colocalized Vti1b with the Golgi resident protein giantin (Linstedt and Hauri

265   1993) and with TGN46 which mainly resides in the TGN (Prescott et al. 1997). As shown in

266   Figure 8 more intense colocalization with both of these Golgi proteins was observed in the Ii

267   KO cells.

268   Vti1b has been reported to be in a complex with other endosomal SNARE proteins

269   (Antonin et al. 2000; Wade et al. 2001; Pryor et al. 2004). However, the colocalization of CI-

270   M6PR with fusion proteins of Vamp7, Stx8 and VAMP8 was not altered in the Ii KO cells (Fig

271   EV1), indicating that the effect of Ii is not general for endosomal SNAREs and possibly specific

272   for Vti1b.

273

274   **Vti1b is expressed in APCs and its protein levels are not affected by Ii expression**

275   Given the important role of Ii in professional APCs and in antigen presentation

276   (reviewed in (Schroder 2016)), we determined Vti1b protein level in APCs and other cell types.

277   The expression levels of Vti1b in monocyte-derived dendritic cells, EBV immortalized B cells,

278   the melanoma cell line MelJuSo, HeLa, Raji, M1 and Neuro2A cells was analysed by Western

279   blot (Fig EV2A). Vti1b was widely expressed (Fig EV2A). To test whether Ii affects the

280   expression levels of this SNARE protein, we analyzed Raji B cells (Fig EV2B,C) or the

281   melanoma cell line MelJuSo (Fig EV2D,E) both wt and Ii KO. In both cell lines the expression

282   of Vti1b was not affected by Ii expression. Similarly, high levels of Ii expression in M1 pMep4-

283   Ii cells after induction with $CdCl_2$ (Fig EV2F) did also not affect Vti1b expression (Fig EV2).

284   Ii expression does not affect endogenous Vti1b expression.

285

286   **Knockdown of Vti1b does not affect lysosome dynamics and expression of endosomal**

287   **marker proteins**

288   Vti1b is reported to be a SNARE mainly involved in the late steps of endocytosis

289   (Antonin et al. 2000; Pryor et al. 2004; Luzio et al. 2009; Kreykenbohm et al. 2002) and we

290   wondered whether Vti1b knock down could affect the expression of other proteins relevant in

291   the endosomal pathway (Rab7a, Rab7b, Rab9, LAMPI and EEA1, see Fig EV3). Western blot

292   analysis revealed that the expression level of these endosomal proteins was unaltered after

293   Vti1b depletion (Fig EV3B-F). In addition, we were also unable to detect significant alterations

9

294 in the endosomal system in the Vti1b depleted M1 cells, even when Ii was expressed (Movie
295 EV1).

296

297 **Silencing of Vti1b abrogates the endosomal maturation delay induced by Ii**

298 Ii expression delays endosomal maturation from early Rab5 positive endosomes to late
299 Rab7 positive endosomes (Gorvel et al. 1995; Landsverk et al. 2011) which correlates to Ii
300 induced endosomal enlargement (Nordeng et al. 2002; Gregers et al. 2003). It would then be
301 imperative that depletion of Vti1b would counteract the Ii induced endosomal maturation delay.
302 The rate of endosomal maturation was determined by colocalization of the fluorescent fluid
303 phase marker dextran-AlexaFluor 488 with Lysotracker Deep Red as a function of time in live
304 cells. When we performed the assay in M1 pMep4-Ii cells without adding $CdCl_2$ and thus not
305 expressing Ii, 65% of dextran was localizing with Lysotracker Deep Red after 1 h. When
306 expression of Ii was induced by $CdCl_2$, entry of dextran was strongly delayed with only 35%
307 overlap after one hour (Fig 9). This again involved Vti1b as silencing of Vti1b before induction
308 of Ii expression restored the Ii delayed rate of endosomal transport and fusion to close to that
309 of the control cells not expressing Ii. This suggests that Vti1b is essential for the Ii induced
310 delay in endosomal maturation.

311

312

313 **Discussion**

314 Invariant chain associates with MHCII and the first function to be described was its
315 ability to sort MHCII molecules to intracellular endosomal compartments. It was later shown
316 that Ii actively sort other molecules to the endosomal pathway such as CD1 and MHCI, both
317 molecules that participates in antigen presentation to specific T cells (for reviews see (Neefjes
318 et al. 2011) and (Schroder 2016)). Other striking trafficking features of Ii is that, when
319 expressed in non-antigen-presenting cells, it delays endosomal maturation (Gorvel et al. 1995;
320 Landsverk et al. 2011). In addition, Ii has "fusogenic" properties as expression in cells lead to
321 homotypic fusion of early endosomes (Nordeng et al. 2002; Romagnoli et al. 1993; Stang and
322 Bakke 1997). This had led to the hypothesis that Ii is a key immunological molecule that is
323 essential for creating "immunoendosomes" suitable for slowly processing endosomal contents
324 for antigen loading (Neefjes et al. 2011). The MHCII-positive multivesicular late endosomal
325 compartment in antigen-presenting cells (Peters et al. 1995) should then be a typical
326 immunoendosome. The idea that Ii may delay endosomal maturation was until now only seen

10

327 in fibroblast cells when transfected with Ii (Gorvel et al. 1995) which may fundamentally differ

328 from professional antigen presenting cells. Here we show that KO of Ii in the antigen-

329 presenting Raji B cell line and the MHCII positive Meljuso cells also affects endosomal

330 maturation, in this case the Ii KO results in faster maturation. No direct correlation has been

331 shown between the Ii induced formation of enlarged early endosomes and Ii induced maturation

332 delay, however, mutations of the charged residues from negative to positive in the cytosolic

333 tail of Ii has been found to abrogate both effects without altering the leucine sorting signals

334 (Gregers et al. 2003; Nordeng et al. 2002) indicating that both effects are caused by similar

335 mechanisms.

336 　　　　How would Ii manipulate the endosomal pathway? We have shown by NMR studies

337 that the cytosolic tails of invariant chain could interact in trans and possibly interact in

338 homotypic fusion (Motta et al. 1997). Ii has a short cytosolic tail of 30 aa, which would prevent

339 it as acting as a genuine SNARE. It is thus more likely that other molecules are recruited to Ii

340 to manipulate the endosomal pathway. We showed earlier that EEA1 or Rab5 were not essential

341 for the Ii induced fusion and resulting enlargement of endosomes (Nordeng et al. 2002).

342 However, the chemical compound NEM, that inhibits the SNARE function blocked fusion and

343 formation of Ii induced enlarged endosomes (Nordeng et al. 2002), bringing our attention to

344 SNAREs as essential for the process. We confirmed this data in the system that we used for the

345 screen (Fig. 2B).

346 　　　　Based on these data we performed an RNAi screen to search for specific SNAREs that

347 were essential for the Ii induced endosomal fusion. In our RNAi screen, we found that silencing

348 of the Qb SNARE, Vti1b strongly decreased Ii-induced endosomal size (Fig 2C-E).

349 Interestingly, although Vti1b has a major role in the fusion of late endosomes, it has not been

350 implicated in the fusion of early endosomes (Luzio et al. 2009; Pryor et al. 2004; Kreykenbohm

351 et al. 2002; Antonin et al. 2000). This shows that Ii employs a SNARE complex that is

352 independent of the canonical early endosomal fusion machinery and can act in parallel.

353 In support of this, enlargement of endosomes induced by the expression of the constitutively

354 active mutant of Rab5, Rab5Q79L, was not affected by Vti1b silencing (Fig 3). Interestingly,

355 the reduction of Ii-positive endosomal size was accompanied by an increase in the number of

356 Ii-positive endosomes, corroborating the hypothesis that Ii-induced enlargement of endosomes

357 is due to an increase in endosomal fusion rather than reduced fission.

358 　　　　In support of this data, we demonstrated that both overexpressed and endogenous Vti1b

359 was localized at the contact sites of Ii-positive endosomes in different cell lines and especially

360 that Vti1b was directly at the opening fusion pore of fusing endosomes (Fig. 4; Movie EV1).

11

361 Strikingly, the effect was highly pronounced for the Ii-enlarged endosomes and Vti1b was

362 detected at 80% of the endosome-endosome contact points. Using another method that enlarges

363 endosomes, the constitutive active Rab5 (Rab5Q79L) (Wegner et al. 2010), Vti1b was only

364 seen in 40% of the contact sites. This indicates that Vti1b is located at the site where fusion is

365 happening and invariant chain expression then affects the location of Vti1b.

366 Immunoprecipitation studies showed that Vti1b binds to Ii, directly or indirectly and this

367 interaction may be the reason for the presence of Vti1b in the contact zone between Ii-positive

368 endosomes. The fact that tailless Ii (Ii Δ27) also co-isolated Vti1b, suggests that the interaction

369 is via their transmembrane domains or indirect.

370   The antigen presenting cell line Meljuso expresses Ii, and we find that the distribution

371 of Vti1b was shifted perinuclear in the Ii KO cells showing an increased colocalization with

372 CI-M6PR, Giantin and TGN46 (Fig. 7,8), which all are located mainly at the Golgi and

373 correspondingly fewer Vti1b-positive vesicles were detected in Ii KO cells (Fig. 7). This

374 suggest that Ii in wt Meljuso cells is involved in transport of Vti1b to the endosomal pathway.

375   Vti1b can move from TGN to late endosomes by binding to the AP1 interactor

376 Clint1/EpsinR (Hirst et al. 2004). Ii, in addition to interacting to AP1, can also interact with

377 AP2, responsible for internalization from the plasma membrane (Kongsvik et al. 2002;

378 Hofmann et al. 1999). Ii is essential for efficient traffic of MHCII to the endosomal pathway

379 and efficient antigen presentation (reviewed in (Neefjes et al. 2011)), but can also deliver other

380 transmembrane proteins to endosomes, including CD70 (Zwart et al. 2010) and the FcR (Ye et

381 al. 2008). We now suggest that Vti1b, due to its interaction with Ii, in antigen-presenting cells

382 is sorted to the early endosomal pathway and thus participates in controlling endosomal

383 maturation and fusion. As silencing of Vti1b leads to less endosomal fusion, we may also

384 postulate that the Vti1b is instrumental for the Ii induced endosomal fusion (Nordeng et al.

385 2002; Romagnoli et al. 1993; Stang and Bakke 1997).

386   We here show that both the fusogenic properties of Ii and the maturation delay depend

387 on the presence of Vti1b as silencing Vti1b corrected the Ii induced maturation delay in M1

388 cells. In this case, increased fusion mediated by Ii and the SNARE Vti1b and possibly other

389 interactors on early endosomes would lead to a prolonged EE phase. Ii is also found to delay

390 protein proteolysis (Gregers et al. 2003; Landsverk et al. 2011) and the part of the endosomal

391 pathway that is trafficked by invariant chain would then create an ideal pathway for

392 proteolytically processing instead of rapidly degrading antigenic proteins for MHC antigen

393 loading of both MHCI, MHCII and CD1 that all associate with Ii.

394   Based on these data, we propose the following model (Fig 10). Ii binds directly or

395   indirectly Vti1b for transport to endosomes, where can then engage in trans-SNARE complex

396   formation. Higher degree of endosomal fusion dependent on a relocation of the "late" SNARE,

397   Vti1b to early endosomes prolongs the EE phase and leads to a slower maturation creating a

398   less proteolytic endosomal pathway. The model further postulate that as Ii positive endosomal

399   vesicles engage in homotypic fusion, then not only Ii but also the associated molecules like

400   MHCII will be concentrated in some late endosomal/lysosomal vesicles as in the MIIC

401   compartment (Peters et al. 1991).

402   It is very interesting that the expression of a single protein, in this case Ii, a protein

403   specific to antigen-presenting cells has the ability to reshape the endosomal pathway in a

404   specific way. Our results support the notion that Ii not only increases the fusion of early

405   endosomes by employing the late endosomal Qb-SNARE Vti1b but also affects endosomal

406   maturation. Therefore, Ii is not only chaperoning MHCII to the loading compartment (MIIC),

407   but is also involved in shaping this specialized organelle of professional APCs. The MIIC has

408   a unique proteolytic environment, less aggressive than that of classical lysosomes (Neefjes

409   1999) which is needed for efficient but not full processing of antigens. We suggest that this

410   property is intricately connected to Ii's ability of delaying endosomal maturation. In addition,

411   the antigen loading compartments integrate antigen input from several other sources than

412   endocytosis, such as phagocytosis, macropinocytosis and autophagy (Blum, Wearsch, and

413   Cresswell 2013), but whether the transfer of these to the immunoendosome is by a general or

414   a more specific mechanism is not known.

415   In conclusion, we show here that the Qb SNARE Vti1b is involved in Ii-mediated

416   endosomal fusion. Ii redistributes Vti1b from the Golgi to early endosomes, which leads to

417   increased fusion and also delayed maturation of endosomes. This mechanism of regulating

418   endosomal fusion could be critical for efficient MHCI and II antigen presentation and thus

419   normal immune responses.

420

421

422

423   **Materials and Methods**

424   **Cell lines**

425   The human fibroblast-like M1 cells (Royer-Pokora, Peterson, and Haseltine 1984) stably

426   transfected with pMep4-Ii (Skjeldal et al. 2012), the human melanoma cell line Meljuso

13

427 (Johnson et al. 1981), the human lymphoblast cell line Raji (Pulvertaft 1964), the human

428 adenocarcinoma HeLa cells (ATCC CCL-2) and the rat neuronal Neuro2A cell line (Cogli et

429 al. 2013) were described before. Healthy donor derived Epstein-Barr virus growth-transformed

430 lymphoblastoid cell lines (EBV-LCL) were provided by Sebastien Wälchli.

431 Mononuclear cells were isolated from buffy-coats from healthy donors through density-

432 gradient centrifugation by using Lymphoprep® (Axis Shield). Buffy-coats from anonymous

433 donors were obtained from the local blood bank (Section for Immunology and Blood

434 Transfusion, Ullevål University Hospital, Oslo, Norway) according to the guidelines of the

435 local blood bank approved by the Norwegian Regional Committee for Medical Research

436 Ethics. Monocyte-derived dendritic cells (MDDCs) were generated from plastic adherent or

437 directly isolated monocytes (Monocyte Isolation Kit II, Miltenyi Biotec) through culture for 6

438 days in Roswell Park Memorial Institute medium (RPMI-1640; (Lonza) containing 100 ng/ml

439 granulocyte-macrophage colony stimulating factor (GM-CSF; Immunotools) and 20 ng/ml IL-

440 4 (Invitrogen, Life Technologies) supplemented with 10% fetal calf serum (FCS), 2 mM L-

441 glutamine, 100 U/ml penicillin and 100 µg/ml streptomycin (Sigma).

442 M1 and HeLa cell lines were grown in Dulbecco's Modified Eagle's Medium (DMEM; Lonza)

443 supplemented with 10% FCS, 2 mM L-glutamine, 100 U/ml penicillin and 100 µg/ml

444 streptomycin (all Sigma). Additionally, 200 µg/ml hygromycin B (Sigma) was added to stably

445 transfected M1 cells. Meljuso, Raji, EBV and MDDCs were grown in RPMI-1640

446 supplemented with 10% FCS, 2 mM L-glutamine, 100 U/ml penicillin and 100 µg/ml

447 streptomycin.

448 For live-cell microscopy, cells were grown in 35mm glass bottom dishes (MatTek), µ-Slide 8

449 Well glass bottom (ibid), or 4-chamber 35mm glass bottom dish (CellVis) for 24 h in complete

450 medium.

451

452 **Establishment of CRISPR/Cas9 Ii KO cell lines**

453 Raji Cas9 and Ii knockout cell lines to be described elsewhere. Meljuso cells were transfected

454 with px330 Sp-Cas9 and sgRNA vectors (12456 and 12458 targeting Ii exon 1) together with

455 a vector coding for blasticidin resistance using Lipofectamine® 2000. Successfully transfected

456 cells were selected by treatment with blasticidin for 1 week. Colonies grown from resistant

457 cells were picked, expanded and screened for Ii knockout by Western blot.

458

459 **Constructs**

14

460   mEGFP-C1 was a gift from Michael Davidson (Addgene plasmid # 54759). His6-Ii p33 wt and

461   His6-Ii Δ27 in pCGFP-EU were purchased from GenScript. pCGFP-EU empty vector has been

462   described before (Kawate and Gouaux 2006). mcherry-Rab5 Q79L has been described before

463   (Bergeland et al. 2008). The Vti1b-mCitrine plasmid was constructed as follows: the coding

464   sequence of human VTI1B was amplified by PCR using 5' and 3' primers containing an EcoRI

465   and   a   BamHI   restriction   site,   respectively.   Forward   primer   was: 5'-

466   AATCAGAATTCATGGCCTCCTCCG-3'.   Reverse   primer   was   5'-

467   CATCGGATCCCAATGGCTGCGAAAGAATTTG-3'. The fragment was then subcloned

468   into pECFP-N1 plasmid cut with EcoRI and BamHI. The identity of all plasmids was

469   confirmed by Sanger sequencing (GATC biotech).

470

471   **Antibodies and reagents**

472   Primary antibodies used were: mouse anti-Ii (clone M-B741, targeting the extracellular/luminal

473   domain, 555538, 1:500) and mouse anti-EEA1 (610456, 1:200 for immunofluorescence;

474   1:1000 for western blot) from BD Biosciences; mouse anti-tubulin (13-8000, 1:12000) from

475   Life Technologies; rabbit anti-Rab7a (2094S, 1:500) from Cell Signaling; rabbit anti-GFP

476   (ab6556, 1:2000), rabbit anti-Vti1b (ab184170, 1:200 for Western blot, 1:100 for

477   immunofluorescence), rabbit anti-CI-M6PR (ab32815, 1:200) and mouse anti-Rab9 (ab2810,

478   1:300) from Abcam; mouse anti-Rab7b (H00338382-M01, 1:300) from Abnova, and mouse

479   anti-LAMP1 (H4A3, 1:500 for immunofluorescence; 1:4000 for western blot) from

480   Developmental Hybridoma Bank. AlexaFluor™ secondary antibodies (Invitrogen) were used

481   for immunofluorescence analysis at 1:200 dilution. Secondary antibodies conjugated with

482   horseradish peroxidase (GE Healthcare) were used at 1:5000 for immunoblotting.

483   Anti-Ii for live immunostaining was labelled using Monoclonal antibody labeling kit

484   (Molecular Probes) according to manufacturer's protocol with AlexaFluor™-488, -555, or -

485   647, respectively.

486   Hoechst dye (H3569, Life Technologies) was used at 0.2 µg/ml. LysoTracker® Red DND-99

487   (LTR), used at a concentration of 100 nM, LysoTracker® DeepRed, used at a concentration of

488   50 nM, 8-Hydroxypyrene-1,3,6-trisulfonic acid trisodium salt (HPTS), used at 1 mM

489   concentration, and dextran AlexaFluor 488 10,000 MW, used at a concentration of 0,5 mg/ml,

490   were purchased from Thermo Fisher.

491   Poly-L-lysine (PLL, 0.01% solution), Wortmannin and N-ethylmaleimide (NEM) were all

492   purchased from Sigma.

493

15

siRNA transfection

Individual siRNAs were transfected by forward transfection using Lipofectamine® RNAiMax reagent (Thermo Fisher) according to manufacturer's protocol. In brief, 250.000 cells/well were seeded in 6-well plates (VWR) in 1 ml antibiotic-free medium 24h prior to transfection. Transfection mixes were prepared by diluting 2.5 µl siRNA stock (80 µM) in 250 µl Opti-MEM and 6 µl RNAiMax in 250 µl Opti-MEM followed by immediate mixing of both. The transfection mixture was then incubated at room temperature for 20 min before addition to the cells. 4h after transfection 1 ml of complete medium was added. Medium on the cells was replaced the next day. 48h after transfections, cells were washed twice with pre-warmed PBS, trypsinized for 1min, resuspended in 2 ml complete medium and split between 35 mm imaging dishes (MatTek) or 8-well slides (ibidi) for imaging and 6-well plates for lysis and subsequent biochemical assays.

Plasmid transfection

For plasmid transfection, cells were transfected using Lipofectamine® 2000 (Thermo Fisher) according to manufacturer's protocol. In brief, cells were seeded the day before transfection. Before transfection, the medium was replaced by Opti-MEM® (Thermo Fisher). Transfection mixes were prepared with 1.5 µl Lipofectamine® 2000 (Thermo Fisher) per 1 µg of plasmid DNA. The transfection mix was then added drop-wise to the cells.

Immunofluorescence

For immunofluorescence, cells were grown on 10x10mm #1.5 high precision coverslips (Marienfeld). Cells were washed twice with ice-cold PBS, fixed at room temperature for 15 min with 3% PFA, quenched for 2 min with 50 mM NH_4Cl, washed again twice with PBS, permeabilized for 15 min with 0.25% saponin (Sigma) in PBS, incubated with primary antibody for 20 min, washed 3 times for 5 min each with 0.1% saponin in PBS, incubated with appropriate secondary antibody for 20 min in the dark, washed three times for 5 min each with 0.1% saponin in PBS, washed twice with PBS, and mounted with mowiol on glass slides (Thermo Scientific).

Endocytic trafficking assay

Cells were grown for 24h on 35mm glass bottom dishes (MatTek) or 35 mm 4-chamber glass bottom dishes (CellVis) in complete medium without phenol red. LTR was added and cells incubated for another 15 min at 37°C before addition of HPTS, 10 min before start of time-

16

528 lapse imaging. For dextran internalization assay, cells have been incubated with 0,5 mg/ml
529 dextran and Lysotracker Deep Red for five minutes. Then, cells have been washed three times
530 and imaged every five minutes.
531

Confocal Imaging

533 For the siRNA screen, imaging was performed on an Olympus FV1000 XV81 confocal laser
534 scanning microscope (inverted) equipped with a UPLSAPO 60x 1.35NA oil immersion
535 objective. Images of cells transfected with individual siRNAs were acquired on a Leica SP8
536 DMi8-CS confocal microscope equipped with a HC PL Apo 40x 1.3NA oil immersion
537 objective.
538 Live imaging of transfected cells and imaging of immunostained cells was performed on a
539 Zeiss LSM880 microscope equipped with a Plan Apo 63x 1.4NA oil immersion objective. Live
540 cells were imaged using Fast AiryScan mode with optimal sampling for super-resolution.
541 Time-lapse imaging to study the trafficking of HPTS to acidic compartments was performed
542 on a Zeiss LSM880 microscope, equipped with a Plan Apo 40x 1.3NA oil immersion objective.
543 Z stacks of 5 slices each were acquired at intervals of 1 µm every 10 min for a total of 200 min
544 at multiple positions. Hardware-based autofocusing (DefiniteFocus.2) was performed at every
545 position and every time-point. Fluorescence emission of HPTS and LTR was separated by
546 linear unmixing based on reference spectra obtained from single stained samples.
547

Image processing and analysis

549 Endosome size was quantified by using ImageJ software. In brief, confocal 3D stacks were
550 maximum projected, in case of EGFP-Rab5Q79L images, the cytosolic background was
551 subtracted by rolling ball background subtraction. The resulting images where then binarized
552 by using a manually adjusted threshold for each image. After that, the images were inverted,
553 morphologically opened, objects split by watershed processing and manual splitting where
554 needed. Finally, the analyse particles function was used to measure all objects. The Feret's
555 diameter was used as the measurement of object size and objects larger than 3 µm were
556 considered enlarged endosomes.
557 LTR colocalization was quantified using the colocalization function in ZEN blue software
558 (Zeiss). In brief, scatter plots were used to define thresholds on the centre z slice for each
559 position. The ratio of overlapped pixels to all LTR-positive pixels was then calculated for all
560 slices of a z stack, summed for each position and compared between conditions using excel
561 software (Microsoft).

17

562

Immunoblotting

563

Cell lysates were subjected to SDS-PAGE followed by blotting onto polyvinylidene fluoride (PVDF) membranes (Millipore), and probed with each primary antibody diluted in 2% blotting-grade non-fat dry milk (BioRad). Next, membranes were incubated with secondary antibodies conjugated to HRP and subsequently with SuperSignal West Femto Maximum Sensitivity Substrate (Thermo Fisher) before digital imaging (Kodak image station 4000R) or Amersham™ ECL Prime Western Blotting Detection Reagent before exposure on Amersham™ Hyperfilm ECL (both GE Healthcare).

571

Statistical analysis

573

If not indicated otherwise, columns and error bars represent the mean ± standard error of the mean (s.e.m.) of at least three independent experiments. Treatments were compared to control using two-tailed Student's t-test, either paired or unpaired as appropriate (excel). Differences were considered statistically significant at $p<0.05$ (indicated by *), $p<0.01$ (**) and $p<0.001$ (***), respectively.

578

Co-Immunoprecipitation

580

Co-Immunoprecipitation experiments using GFP-trap® (ChromoTek) were performed according to manufacturer's protocol. In brief, $1-2\times10^6$ cells were seeded on 10 cm cell culture dishes and incubated for 24 h at 37°C, 5% CO_2. The cells were then transfected using Lipofectamine 2000 as described earlier. M1 pMep4-Ii cells were treated with 7 µM $CdCl_2$ overnight to induce expression of Ii. Cells were washed twice with ice-cold PBS and lysed in 200 µl lysis buffer (100 mM NaCl, 1 mM EDTA, Complete® protease inhibitors (Sigma), 1 mM PMSF (Phenylmethylsulfonylfluorid, Sigma), 0.5% NP-40) for 30 min on ice. Lysates were cleared by centrifugation at 13,000 x g for 10 min at 4°C, diluted with 300 µl buffer and loaded on magnetic agarose anti-GFP beads (GFP-trap®_MA, ChromoTek) for 1 h at 4°C. Beads were then washed three times. Proteins were eluted using 2x Laemmli sample buffer with freshly added D-thiotreitol (200 mM, Sigma) for 10 min at 95°C.

591

595 State University) for providing the mEGFP-C1plasmid through Addgene and Jens P. Morth

596 (University of Oslo) for the pCGFP-EU empty vector. Finally, we thank the NorMIC Oslo

597 imaging platform, Department of Biosciences, University of Oslo.

598 We gratefully acknowledge the support from the Research Council of Norway (Grants 214183,

599 and 230770 to OB) and the Norwegian Cancer Society (grant 113472 to OB).

600

Author contributions

602 DF and AM designed, performed, analyzed the majority of the experiments, MD contributed

603 to the IP experiments and WB experiment in different cell types. LJ and JN generated the

604 Meljuso Ii knock-out cell line, MM and JT generated the Raji Ii knock-out cell line. OB

605 coordinated the project and DF, AM and OB wrote the manuscript. All co-authors approved

606 the final version of the manuscript.

607

Conflict of interest

609 The authors declare no conflict of interest.

610

References

612

613 Antonin, W., C. Holroyd, D. Fasshauer, S. Pabst, G. F. Von Mollard, and R. Jahn. 2000. 'A
614   SNARE complex mediating fusion of late endosomes defines conserved properties of
615   SNARE structure and function', *EMBO J*, 19: 6453-64.
616 Bakke, O., and B. Dobberstein. 1990. 'MHC class II-associated invariant chain contains a
617   sorting signal for endosomal compartments', *Cell*, 63: 707-16.
618 Bergeland, T., L. Haugen, O. J. Landsverk, H. Stenmark, and O. Bakke. 2008. 'Cell-cycle-
619   dependent binding kinetics for the early endosomal tethering factor EEA1', *EMBO Rep*,
620   9: 171-8.
621 Bikoff, E. K., L. Y. Huang, V. Episkopou, J. van Meerwijk, R. N. Germain, and E. J. Robertson.
622   1993. 'Defective major histocompatibility complex class II assembly, transport, peptide
623   acquisition, and CD4+ T cell selection in mice lacking invariant chain expression', *J
624   Exp Med*, 177: 1699-712.
625 Blum, J. S., P. A. Wearsch, and P. Cresswell. 2013. 'Pathways of antigen processing', *Annu
626   Rev Immunol*, 31: 443-73.
627 Bremnes, B., T. Madsen, M. Gedde-Dahl, and O. Bakke. 1994. 'An LI and ML motif in the
628   cytoplasmic tail of the MHC-associated invariant chain mediate rapid internalization', *J
629   Cell Sci*, 107 (Pt 7): 2021-32.
630 Brunger, A. T. 2005. 'Structure and function of SNARE and SNARE-interacting proteins', *Q
631   Rev Biophys*, 38: 1-47.
632 Cogli, L., C. Progida, C. L. Thomas, B. Spencer-Dene, C. Donno, G. Schiavo, and C. Bucci.
633   2013. 'Charcot-Marie-Tooth type 2B disease-causing RAB7A mutant proteins show
634   altered interaction with the neuronal intermediate filament peripherin', *Acta
635   Neuropathol*, 125: 257-72.

636 Cuenda, A., J. Rouse, Y. N. Doza, R. Meier, P. Cohen, T. F. Gallagher, P. R. Young, and J.
637   C. Lee. 1995. 'SB 203580 is a specific inhibitor of a MAP kinase homologue which is
638   stimulated by cellular stresses and interleukin-1', *FEBS Lett*, 364: 229-33.
639 Elliott, E. A., J. R. Drake, S. Amigorena, J. Elsemore, P. Webster, I. Mellman, and R. A. Flavell.
640   1994. 'The invariant chain is required for intracellular transport and function of major
641   histocompatibility complex class II molecules', *J Exp Med*, 179: 681-94.
642 Elliott, T., and J. Neefjes. 2006. 'The complex route to MHC class I-peptide complexes', *Cell*,
643   127: 249-51.
644 Fasshauer, D., R. B. Sutton, A. T. Brunger, and R. Jahn. 1998. 'Conserved structural features
645   of the synaptic fusion complex: SNARE proteins reclassified as Q- and R-SNAREs',
646   *Proc Natl Acad Sci U S A*, 95: 15781-6.
647 Genuardi, M., and G. F. Saunders. 1988. 'Localization of the HLA class II-associated invariant
648   chain gene to human chromosome band 5q32', *Immunogenetics*, 28: 53-6.
649 Gorvel, J. P., J. M. Escola, E. Stang, and O. Bakke. 1995. 'Invariant chain induces a delayed
650   transport from early to late endosomes', *J Biol Chem*, 270: 2741-6.
651 Gregers, T. F., T. W. Nordeng, H. C. Birkeland, I. Sandlie, and O. Bakke. 2003. 'The
652   cytoplasmic tail of invariant chain modulates antigen processing and presentation', *Eur
653   J Immunol*, 33: 277-86.
654 Haugen, L. H., F. M. Skjeldal, T. Bergeland, and O. Bakke. 2017. 'Endosomal binding kinetics
655   of Eps15 and Hrs specifically regulate the degradation of RTKs', *Sci Rep*, 7: 17962.
656 Hille-Rehfeld, A. 1995. 'Mannose 6-phosphate receptors in sorting and transport of lysosomal
657   enzymes', *Biochim Biophys Acta*, 1241: 177-94.
658 Hirst, J., S. E. Miller, M. J. Taylor, G. F. von Mollard, and M. S. Robinson. 2004. 'EpsinR is an
659   adaptor for the SNARE protein Vti1b', *Mol Biol Cell*, 15: 5593-602.
660 Hofmann, M. W., S. Honing, D. Rodionov, B. Dobberstein, K. von Figura, and O. Bakke. 1999.
661   'The leucine-based sorting motifs in the cytoplasmic domain of the invariant chain are
662   recognized by the clathrin adaptors AP1 and AP2 and their medium chains', *J Biol
663   Chem*, 274: 36153-8.
664 Jahn, R., and R. H. Scheller. 2006. 'SNAREs--engines for membrane fusion', *Nat Rev Mol Cell
665   Biol*, 7: 631-43.
666 Johnson, J. P., M. Demmer-Dieckmann, T. Meo, M. R. Hadam, and G. Riethmuller. 1981.
667   'Surface antigens of human melanoma cells defined by monoclonal antibodies. I.
668   Biochemical characterization of two antigens found on cell lines and fresh tumors of
669   diverse tissue origin', *Eur J Immunol*, 11: 825-31.
670 Jones, A. T., and M. J. Clague. 1995. 'Phosphatidylinositol 3-kinase activity is required for
671   early endosome fusion', *Biochem J*, 311 (Pt 1): 31-4.
672 Kawate, T., and E. Gouaux. 2006. 'Fluorescence-detection size-exclusion chromatography for
673   precrystallization screening of integral membrane proteins', *Structure*, 14: 673-81.
674 Kongsvik, T. L., S. Honing, O. Bakke, and D. G. Rodionov. 2002. 'Mechanism of interaction
675   between leucine-based sorting signals from the invariant chain and clathrin-associated
676   adaptor protein complexes AP1 and AP2', *J Biol Chem*, 277: 16484-8.
677 Kreykenbohm, V., D. Wenzel, W. Antonin, V. Atlachkine, and G. F. von Mollard. 2002. 'The
678   SNAREs vti1a and vti1b have distinct localization and SNARE complex partners', *Eur
679   J Cell Biol*, 81: 273-80.
680 Landsverk, O. J., O. Bakke, and T. F. Gregers. 2009. 'MHC II and the endocytic pathway:
681   regulation by invariant chain', *Scand J Immunol*, 70: 184-93.
682 Landsverk, O. J., N. Barois, T. F. Gregers, and O. Bakke. 2011. 'Invariant chain increases the
683   half-life of MHC II by delaying endosomal maturation', *Immunol Cell Biol*, 89: 619-29.
684 Linstedt, A. D., and H. P. Hauri. 1993. 'Giantin, a novel conserved Golgi membrane protein
685   containing a cytoplasmic domain of at least 350 kDa', *Mol Biol Cell*, 4: 679-93.
686 Luzio, J. P., M. D. Parkinson, S. R. Gray, and N. A. Bright. 2009. 'The delivery of endocytosed
687   cargo to lysosomes', *Biochem Soc Trans*, 37: 1019-21.
688 Motta, A., P. Amodeo, P. Fucile, M. A. Castiglione Morelli, B. Bremnes, and O. Bakke. 1997.
689   'A new triple-stranded alpha-helical bundle in solution: the assembling of the cytosolic
690   tail of MHC-associated invariant chain', *Structure*, 5: 1453-64.

691 Neefjes, J. 1999. 'CIIV, MIIC and other compartments for MHC class II loading', *Eur J Immunol*,
692   29: 1421-5.
693 Neefjes, J. J., and H. L. Ploegh. 1992. 'Inhibition of endosomal proteolytic activity by leupeptin
694   blocks surface expression of MHC class II molecules and their conversion to SDS
695   resistance alpha beta heterodimers in endosomes', *EMBO J*, 11: 411-6.
696 Neefjes, J., M. L. Jongsma, P. Paul, and O. Bakke. 2011. 'Towards a systems understanding
697   of MHC class I and MHC class II antigen presentation', *Nat Rev Immunol*, 11: 823-36.
698 Nordeng, T. W., T. F. Gregers, T. L. Kongsvik, S. Meresse, J. P. Gorvel, F. Jourdan, A. Motta,
699   and O. Bakke. 2002. 'The cytoplasmic tail of invariant chain regulates endosome fusion
700   and morphology', *Mol Biol Cell*, 13: 1846-56.
701 Peters, P. J., J. J. Neefjes, V. Oorschot, H. L. Ploegh, and H. J. Geuze. 1991. 'Segregation of
702   MHC class II molecules from MHC class I molecules in the Golgi complex for transport
703   to lysosomal compartments', *Nature*, 349: 669-76.
704 Peters, P. J., G. Raposo, J. J. Neefjes, V. Oorschot, R. L. Leijendekker, H. J. Geuze, and H.
705   L. Ploegh. 1995. 'Major histocompatibility complex class II compartments in human B
706   lymphoblastoid cells are distinct from early endosomes', *J Exp Med*, 182: 325-34.
707 Pieters, J., O. Bakke, and B. Dobberstein. 1993. 'The MHC class II-associated invariant chain
708   contains two endosomal targeting signals within its cytoplasmic tail', *J Cell Sci*, 106 (Pt
709   3): 831-46.
710 Powis, G., R. Bonjouklian, M. M. Berggren, A. Gallegos, R. Abraham, C. Ashendel, L. Zalkow,
711   W. F. Matter, J. Dodge, G. Grindey, and et al. 1994. 'Wortmannin, a potent and
712   selective inhibitor of phosphatidylinositol-3-kinase', *Cancer Res*, 54: 2419-23.
713 Prescott, A. R., J. M. Lucocq, J. James, J. M. Lister, and S. Ponnambalam. 1997. 'Distinct
714   compartmentalization of TGN46 and beta 1,4-galactosyltransferase in HeLa cells', *Eur
715   J Cell Biol*, 72: 238-46.
716 Pryor, P. R., B. M. Mullock, N. A. Bright, M. R. Lindsay, S. R. Gray, S. C. Richardson, A.
717   Stewart, D. E. James, R. C. Piper, and J. P. Luzio. 2004. 'Combinatorial SNARE
718   complexes with VAMP7 or VAMP8 define different late endocytic fusion events', *EMBO
719   Rep*, 5: 590-5.
720 Pulvertaft, J. V. 1964. 'Cytology of Burkitt's Tumour (African Lymphoma)', *Lancet*, 1: 238-40.
721 Roche, P. A., C. L. Teletski, E. Stang, O. Bakke, and E. O. Long. 1993. 'Cell surface HLA-DR-
722   invariant chain complexes are targeted to endosomes by rapid internalization', *Proc
723   Natl Acad Sci U S A*, 90: 8581-5.
724 Romagnoli, P., C. Layet, J. Yewdell, O. Bakke, and R. N. Germain. 1993. 'Relationship
725   between invariant chain expression and major histocompatibility complex class II
726   transport into early and late endocytic compartments', *J Exp Med*, 177: 583-96.
727 Royer-Pokora, B., W. D. Peterson, Jr., and W. A. Haseltine. 1984. 'Biological and biochemical
728   characterization of an SV40-transformed xeroderma pigmentosum cell line', *Exp Cell
729   Res*, 151: 408-20.
730 Sand, K. M., O. J. Landsverk, A. Berg-Larsen, O. Bakke, and T. F. Gregers. 2014. 'The human-
731   specific invariant chain isoform Iip35 modulates Iip33 trafficking and function', *Immunol
732   Cell Biol*, 92: 791-8.
733 Schroder, B. 2016. 'The multifaceted roles of the invariant chain CD74--More than just a
734   chaperone', *Biochim Biophys Acta*, 1863: 1269-81.
735 Skjeldal, F. M., S. Strunze, T. Bergeland, E. Walseng, T. F. Gregers, and O. Bakke. 2012.
736   'The fusion of early endosomes induces molecular-motor-driven tubule formation and
737   fission', *J Cell Sci*, 125: 1910-9.
738 Stang, E., and O. Bakke. 1997. 'MHC class II-associated invariant chain-induced enlarged
739   endosomal structures: a morphological study', *Exp Cell Res*, 235: 79-92.
740 Stenmark, H., R. G. Parton, O. Steele-Mortimer, A. Lutcke, J. Gruenberg, and M. Zerial. 1994.
741   'Inhibition of rab5 GTPase activity stimulates membrane fusion in endocytosis', *EMBO
742   J*, 13: 1287-96.
743 Wade, N., N. J. Bryant, L. M. Connolly, R. J. Simpson, J. P. Luzio, R. C. Piper, and D. E.
744   James. 2001. 'Syntaxin 7 complexes with mouse Vps10p tail interactor 1b, syntaxin 6,

745   vesicle-associated membrane protein (VAMP)8, and VAMP7 in b16 melanoma cells',
746   *J Biol Chem*, 276: 19820-7.

747   Wegner, C. S., L. Malerod, N. M. Pedersen, C. Progida, O. Bakke, H. Stenmark, and A. Brech.
748   2010. 'Ultrastructural characterization of giant endosomes induced by GTPase-
749   deficient Rab5', *Histochem Cell Biol*, 133: 41-55.

750   Weimbs, T., S. H. Low, S. J. Chapin, K. E. Mostov, P. Bucher, and K. Hofmann. 1997. 'A
751   conserved domain is present in different families of vesicular fusion proteins: a new
752   superfamily', *Proc Natl Acad Sci U S A*, 94: 3046-51.

753   Wymann, M. P., G. Bulgarelli-Leva, M. J. Zvelebil, L. Pirola, B. Vanhaesebroeck, M. D.
754   Waterfield, and G. Panayotou. 1996. 'Wortmannin inactivates phosphoinositide 3-
755   kinase by covalent modification of Lys-802, a residue involved in the phosphate
756   transfer reaction', *Mol Cell Biol*, 16: 1722-33.

757   Ye, L., X. Liu, S. N. Rout, Z. Li, Y. Yan, L. Lu, T. Kamala, N. K. Nanda, W. Song, S. K. Samal,
758   and X. Zhu. 2008. 'The MHC class II-associated invariant chain interacts with the
759   neonatal Fc gamma receptor and modulates its trafficking to endosomal/lysosomal
760   compartments', *J Immunol*, 181: 2572-85.

761   Zwart, W., V. Peperzak, E. de Vries, A. M. Keller, G. van der Horst, E. A. Veraar, U. Geumann,
762   H. Janssen, L. Janssen, S. H. Naik, J. Neefjes, and J. Borst. 2010. 'The invariant chain
763   transports TNF family member CD70 to MHC class II compartments in dendritic cells',
764   *J Cell Sci*, 123: 3817-27.

765

766

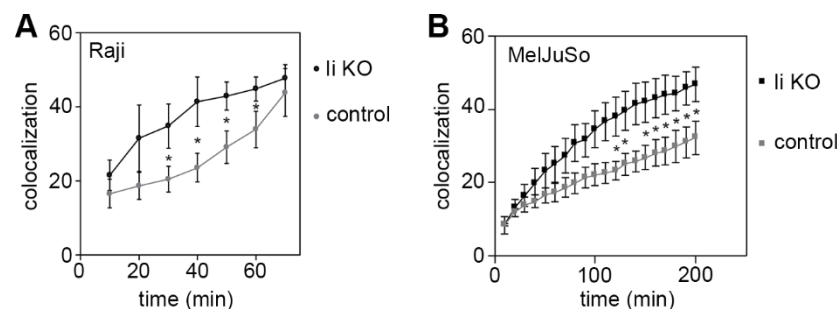767 **Figures and Figure Legends**

768

Figure 1

769

770 **Figure 1. Ii KO speeds up trafficking of HPTS.** A) The colocalization coefficient (% pixel

771 overlap of LysoTracker Red with HPTS) in wt Raji cells expressing Cas9 (control) or Ii

772 knockout (Ii KO) was analysed and is represented by line graphs for control (●) and Ii KO (●)

773 indicating mean ± SEM of 6 independent experiments. B) Same as for A) in wt Meljuso cells

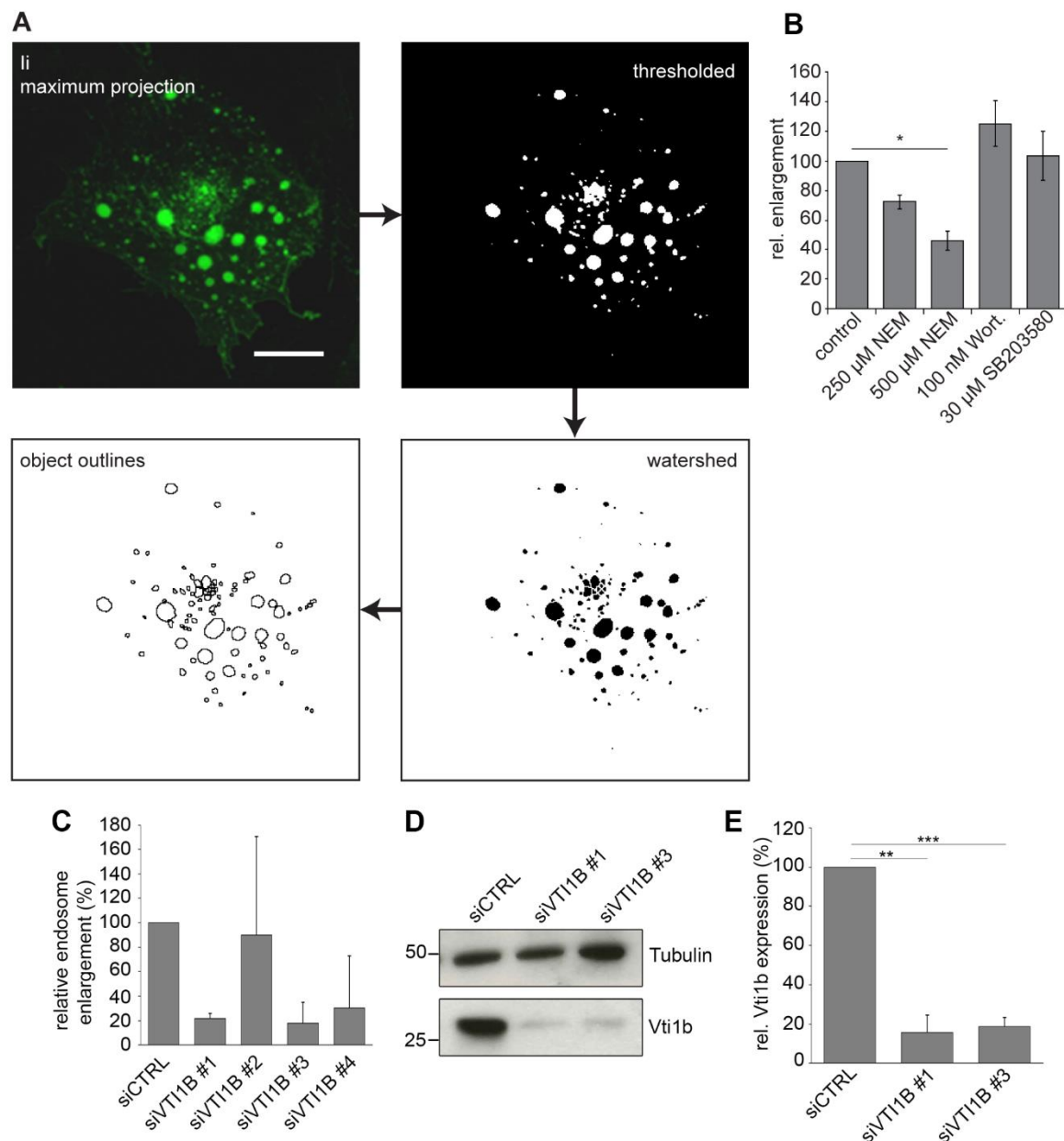774 (control, ●) or Ii KO (●) in showing mean ± SEM for 3 independent experiments.

775

Figure 2

776

Figure 2. Ii-induced enlargement of endosomes is dependent of Vti1b. A) Workflow diagram of the image processing for the quantification of endosome size. Scale bar: 10 µm. C) Results of endosome quantification after treatment with different drugs affecting early endosome fusion, mean ± s.e.m. of three independent experiments. D) Quantifications results of enlarged endosomes (bigger than 3 µm in diameter) for four individual oligonucleotides targeting Vti1b compared to control siRNA (non-targeting, siCTRL) reported as relative endosome enlargement. E) M1-pMep4-Ii cells transfected with control siRNA or siRNA against Vti1b were lysed and subjected to western blot analysis using anti-Vti1b and anti-

23

785   tubulin antibodies. Detection of tubulin has been used as loading control. F) Quantification of

786   Vti1b abundance is shown. Data represent the mean ± s.e.m. of three independent experiments.

787

788

Figure 3

789
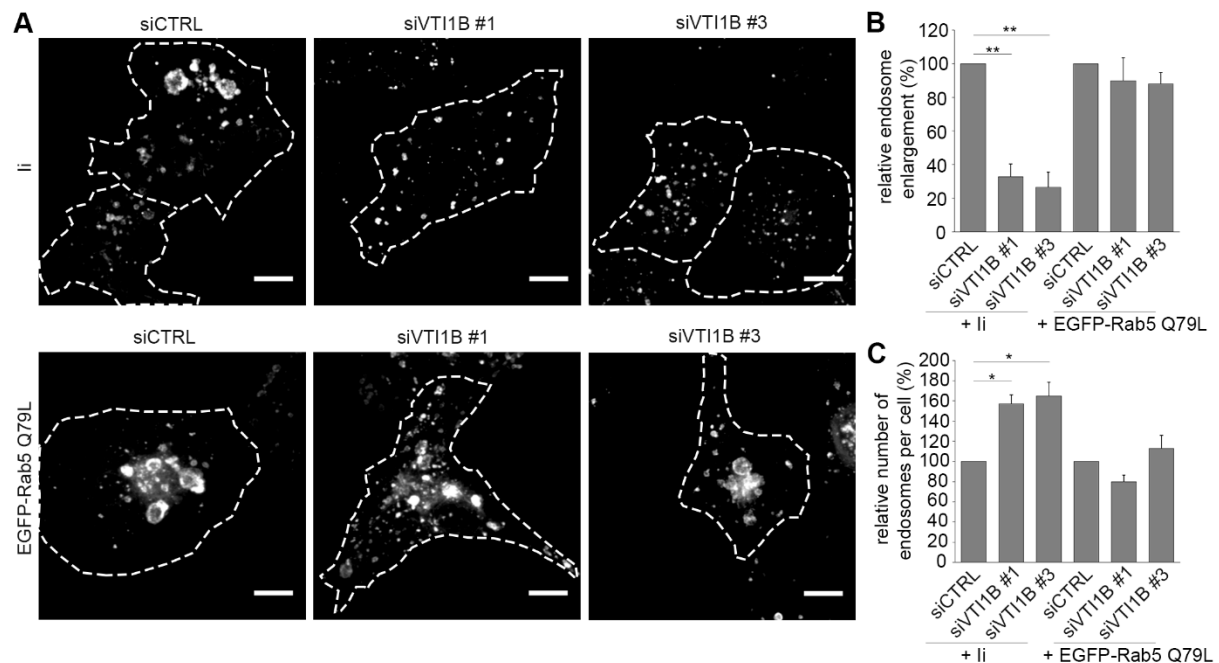
790   **Figure 3. Vti1b specifically reduce Ii-mediated endosome enlargement.** A) M1-pMep4-Ii

791   cells were transfected with control siRNA (siCTRL) or siRNAs targeting VTI1B (siVTI1B #1

792   and siVTI1B #3). After 48h of transfection cells were either treated overnight with 7µM CdCl$_2$

793   to induce Ii expression (top row) or transfected with EGFP-Rab5Q79L (bottom row) as

794   indicated. Cells expressing Ii have been treated with anti-Ii antibody coupled with an Alexa

795   Fluor 488 fluorescent dye for 30 minutes before fixation and imaging. Confocal images are

796   shown. Dashed lines indicate the shape of the cells. Scale bars: 10 µm. B) Quantification of the

797   percentage of endosomes (diameter ≥3 µm) in control and Vti1b silenced cells expressing either

798   Ii or EGFP-Rab5Q79L. Data represent the mean ± s.e.m. of three different experiments (n=50).

799   C) Quantification of the number of endosomes per cell in control and Vti1b silenced cells

800   expressing either Ii or Rab5Q79L. Data represent the mean ± s.e.m. of three different
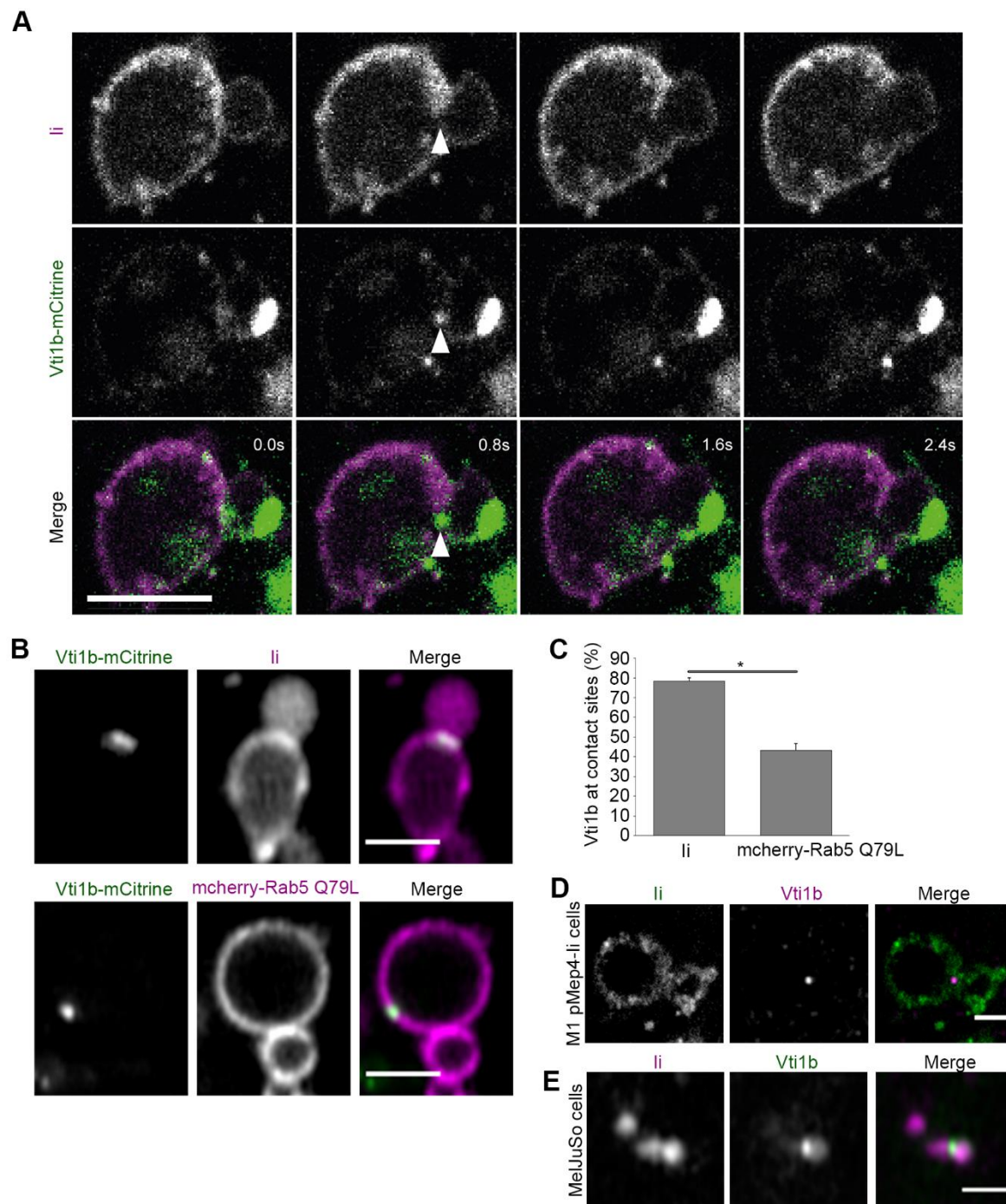
801   experiments.

802

24

Figure 4

803

Figure 4. Vti1b localizes to contact sites at Ii-positive endosomes during fusion. A) M1
pMep4-Ii cells were transiently transfected with Vti1b-mCitrine o/n and Ii was expressed for 8
h (7µM CdCl₂ added). Cells were treated with anti-Ii antibody coupled with Alexa Fluor 647
for 1 hour before live imaging. Time-lapse confocal images of Ii (magenta) and Vti1b-mCitrine
(green) during endosome fusion are shown. Scale bar: 2 µm. B) M1 pMep4-Ii cells were either
transiently transfected with Vti1b-mCitrine and treated with 7µM CdCl₂ for 8h to induce Ii

25

810 expression (top row) or co-transfected with Vti1b-mCitrine and mCherry-Rab5Q79L (bottom

811 row). Cells expressing Ii were treated with anti-Ii antibody coupled with an Alexa Fluor 647

812 fluorescent dye antibody for 1 hour before imaged live by Fast AiryScan. Scale bar: 2 µm. C)

813 Quantification of the percentage of Vti1b localized at the contact sites in cells expressing also

814 Ii or Rab5Q79L as indicated is shown. Data represent the mean ± SEM of three independent

815 experiments. D) M1 pMep4-Ii cells were treated with 7 µM $CdCl_2$ for 8 h to induce Ii

816 expression. Cells were treated with anti-Ii antibody coupled with an Alexa Fluor 647

817 fluorescent dye for 1 hour before fixation and immunostaining for Vti1b. Representative

818 images of Ii (green) and endogenous Vti1b (magenta) positive endosomes are shown. Scale

819 bars: 2 µm. E) Meljuso cells were treated with anti-Ii antibody coupled with an Alexa Fluor

820 647 fluorescent dye for 4 hours before fixation and immunostaining for Vti1b. Representative

821 images of Ii (magenta) and endogenous Vti1b (green) positive endosomes are shown. Scale
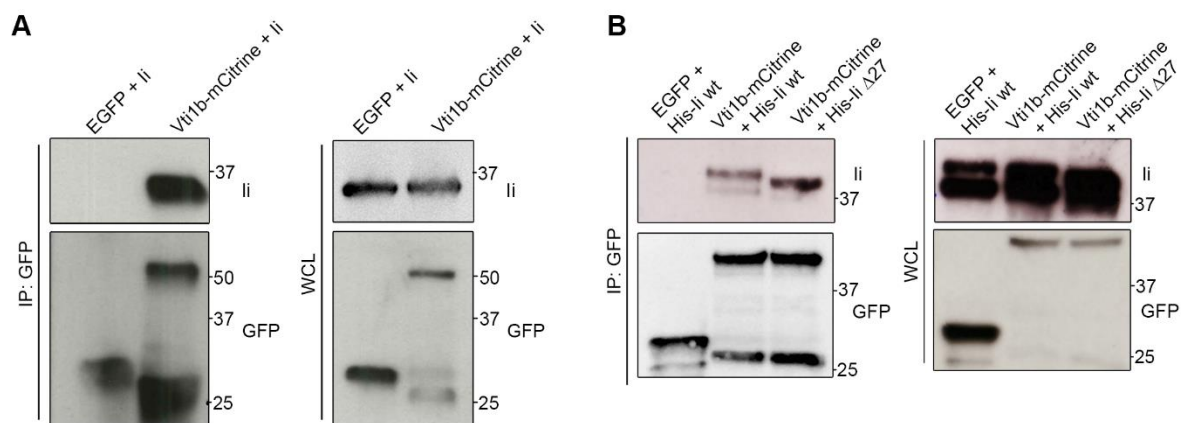
822 bar: 1 µm.

823

824

Figure 5

825 **Figure 5. Vti1b interacts with Ii.** A) M1-pMep4-Ii wt cells were transiently transfected with

826 EGFP or Vti1b-mCitrine and Ii expression was induced by treatment with $CdCl_2$ overnight.

827 Cells were lysed and co-IP with GFP-Trap magnetic beads. Whole-cell lysates (WCL, on the

828 right) and immunoprecipitated (IP, on the left) were subjected to Western blot analysis. B)

829 HeLa cells were transiently co-transfected with either EGFP or Vti1b-mCitrine and Ii wt or

830 mutated as indicated in the figure. Cells were lysed after 24 hours of transfection and thereafter

831 co-IP with GFP-Trap magnetic beads. Whole-cell lysates (WCL, on the right) and

832 immunoprecipitates (IP, on the left) were subjected to Western blot analysis. GFP and Ii was

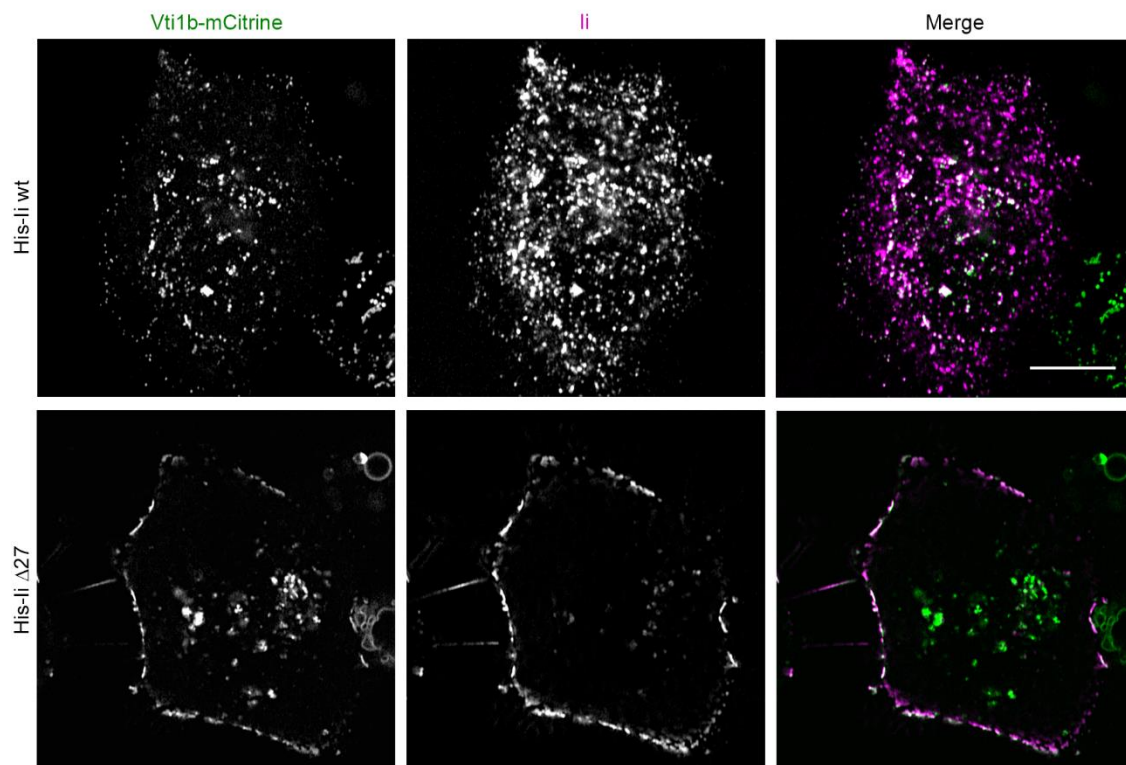833 visualized using the corresponding anti-GFP or anti-Ii antibodies.

26

834

Figure 6

835

836 **Figure 6. Vti1b and Ii Δ27 colocalize at the plasma membrane.** HeLa cells were transfected

837 with Vti1b-mCitrine and His-Ii (wt or Δ27) as indicated in the figure and then imaged. Confocal
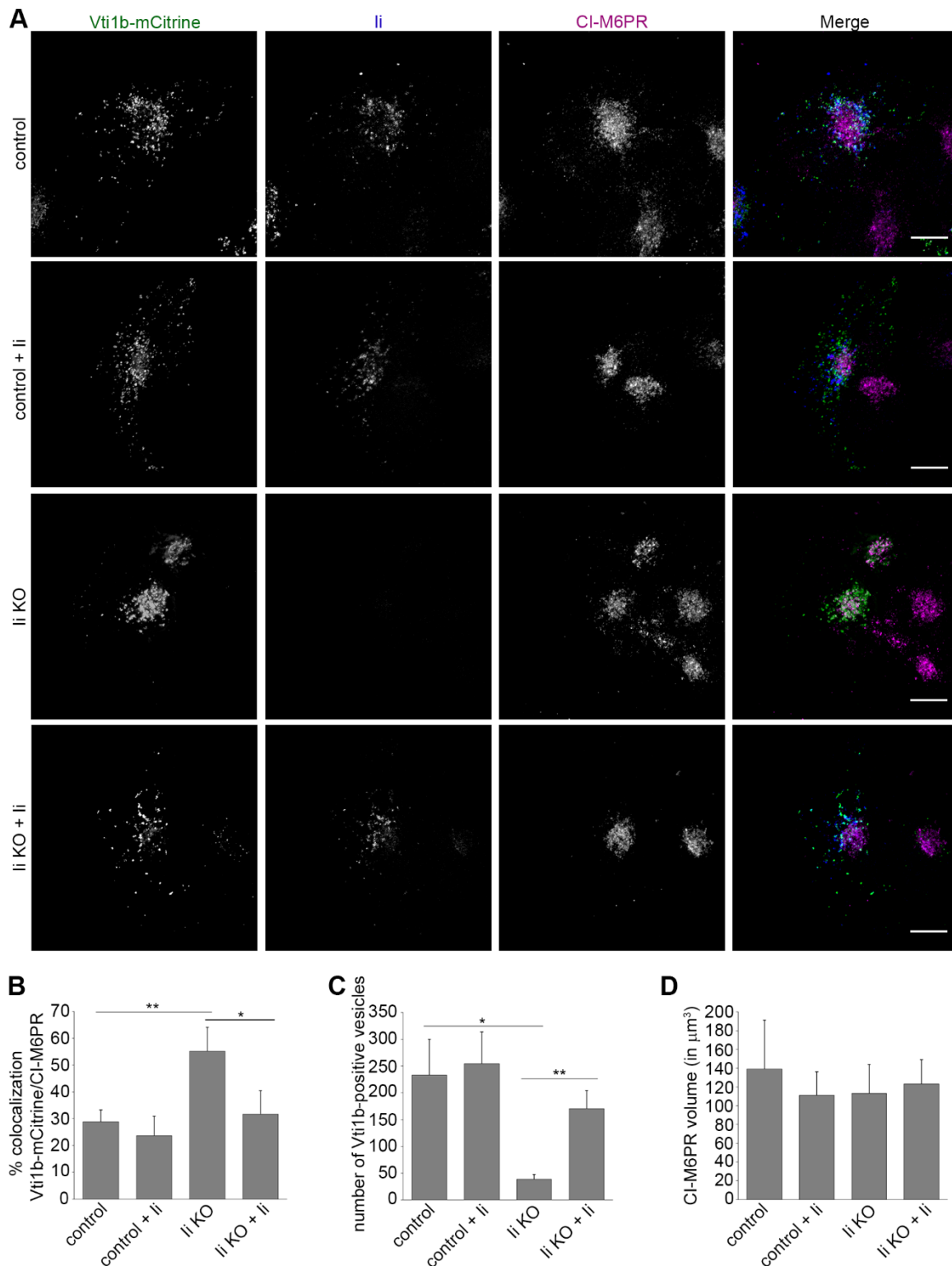
838 images are shown. Scale bar: 10 µm.

839

Figure 7

840

Figure 7. Vti1b localization is altered in Meljuso Ii KO cells. A) Meljuso control and Ii KO cells were transfected with either Vti1b-mCitrine alone or Vti1b-mCitrine and His-Ii as indicated in the figure and subsequently labelled live for Ii by treating the cells with an anti-Ii

844   antibody coupled with an Alexa Fluor 647 for 4 h. Cells were stained after fixation with an

845   anti-CI-M6PR antibody. Representative images (maximal projections) of Vti1b-mCitrine

846   (green), Ii (blue), CI-M6PR (magenta) and merge are shown. Scale bars: 10 µm. B)

847   Quantification of the percentage of colocalization between Vti1b-mCitrine and CI-M6PR in

848   control, Ii-overexpressing, Ii KO or Ii-transfected Ii KO cells is shown. C) Quantification of

849   the number of vesicles per cell positive for Vti1b-mCitrine in control, Ii-overexpressing, Ii KO

850   or Ii-transfected Ii KO cells. D) Quantification of the volume of CI-M6PR positive structure in

851   the indicated samples. Data represent the mean ± SEM of at least three independent
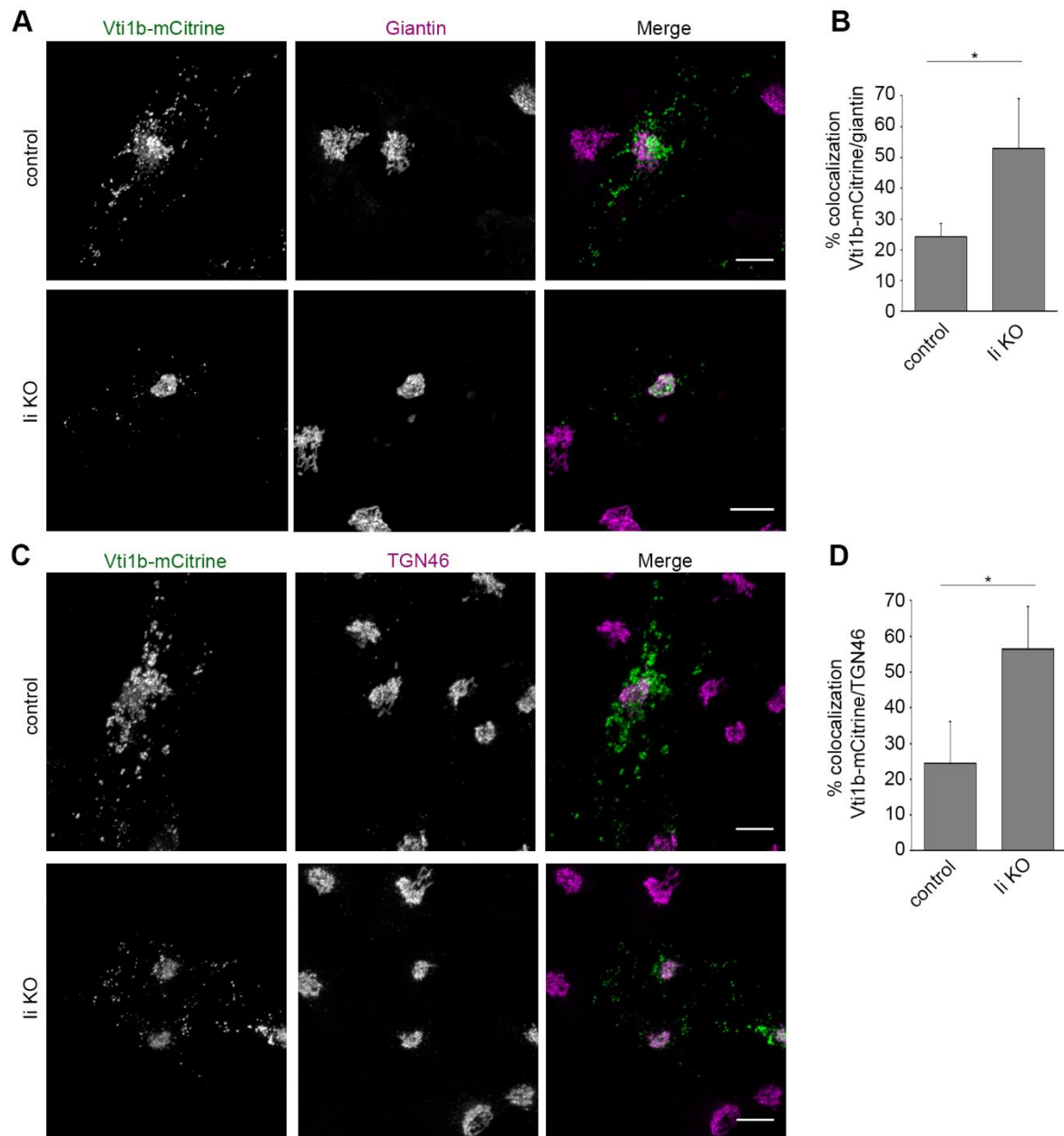
852   experiments.

853

Figure 8

854

Figure 8. Vti1b is more localized on giantin and TGN46 positive structures in Meljuso Ii KO cells. A) Meljuso control and Ii KO cells were transfected with Vti1b-mCitrine and subsequently stained after fixation with an anti-giantin antibody. Representative images (maximal projections) of Vti1b-mCitrine (green), giantin (magenta) and merge are shown. Scale bars: 10 µm. B) Quantification of the percentage of colocalization between Vti1b-mCitrine and giantin in control and Ii KO cells is shown. C) Meljuso control and Ii KO cells were transfected with Vti1b-mCitrine and subsequently stained after fixation and permeabilization with an anti-TGN46 antibody. Representative images (maximal projections) of Vti1b-mCitrine (green), TGN46 (magenta) and merge are shown. Scale bars: 10 µm. B)

30

864   Quantification of the percentage of colocalization between Vti1b-mCitrine and TGN46 in

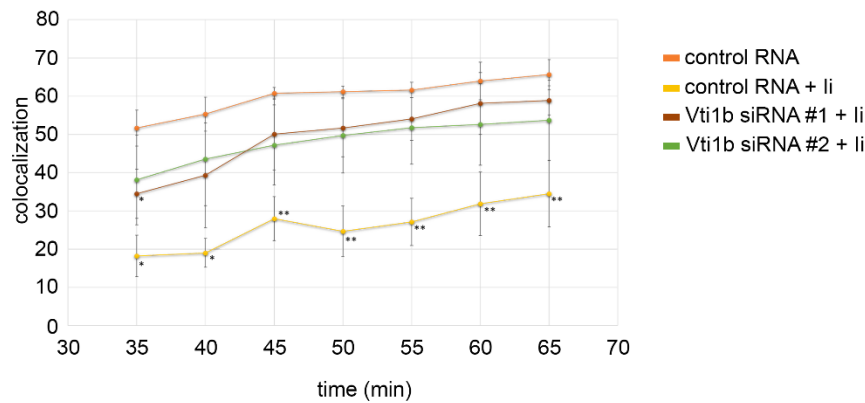865   control and Ii KO cells is shown.

866

867

868

Figure 9

869

870   **Figure 9. Ii causes a delay in trafficking dependent on Vti1b.**

871   Colocalization of dextran and Lysotracker Deep Red in M1-pMep4-Ii cells expressing or not

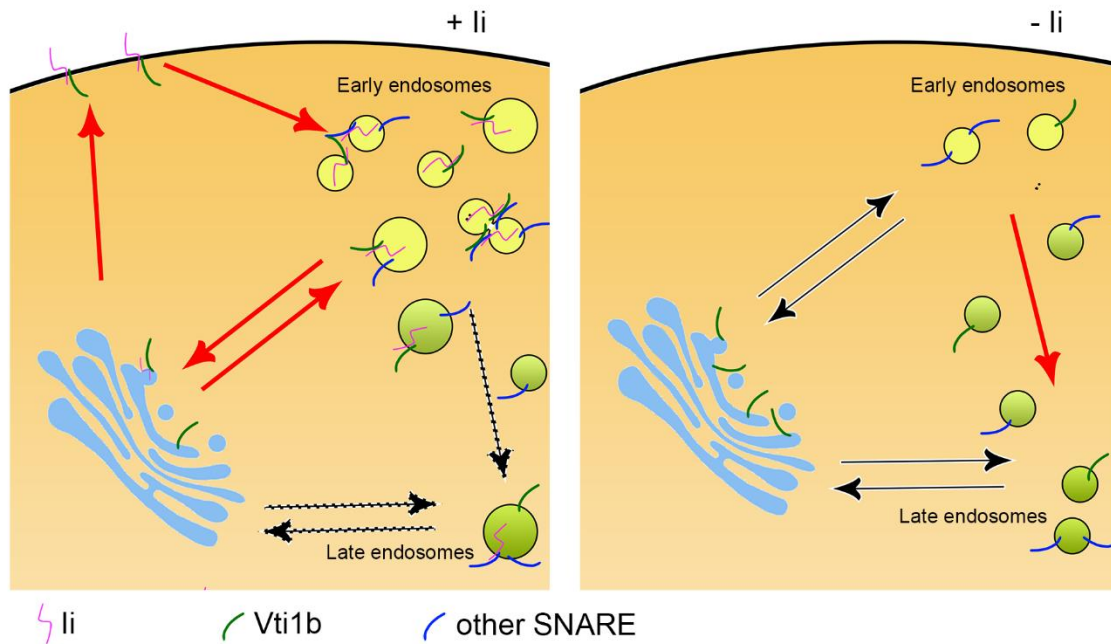872   Ii and treated with control siRNA or siRNAs against VTI1B as indicated.

873

Figure 10

Figure 10. Schematic model depicting the main findings of this study. Ii binds to Vti1b and facilitates its trafficking via the Golgi apparatus to the plasma membrane and from there to early endosomes. There, Vti1b forms a SNARE complex leading to membrane fusion. Increased endosomal fusion dependent on Vti1b delays endosomal maturation (left). Lack of Ii induces a reduction of the endosomal localization of Vti1b, less endosomal fusion and faster endosomal maturation (right).